Velocity measurement in turbulent boundary layer of drag-reducing surfactant solution

Motoyuki Itoh[a)]
Graduate School of Engineering, Nagoya Institute of Technology, Gokiso-cho, Showa-ku, Nagoya, Aichi 466-8555, Japan

Shinji Tamano
Graduate School of Engineering, Nagoya Institute of Technology, Gokiso-cho, Showa-ku, Nagoya, Aichi 466-8555, Japan

Kazuhiko Yokota
Graduate School of Engineering, Nagoya Institute of Technology, Gokiso-cho, Showa-ku, Nagoya, Aichi 466-8555, Japan

Masato Ninagawa
Toyota Motor Corporation, 1 Toyota-cho, Toyota, Aichi 471-8571, Japan

(Received 4 February 2005; accepted 31 May 2005; published online 6 July 2005)

The influence of a drag-reducing surfactant on a zero-pressure gradient turbulent boundary layer was investigated using a two-component laser-Doppler velocimetry system. It was discovered that the streamwise turbulence intensity has a maximum near the center of the boundary layer in addition to the near-wall maximum which appears in canonical wall-bounded turbulent flow. At the location of the additional maximum, the Reynolds shear stress has a slight maximum, the skewness factor of streamwise turbulent fluctuation is zero, and the flatness factor has a minimum. © *2005 American Institute of Physics*. [DOI: 10.1063/1.1979523]

I. INTRODUCTION

It is well known that a drag reduction of up to 80% can be achieved by the addition of a small amount of a surfactant or polymer into a wall-bounded turbulent flow.[1,2] As well as experimental studies on turbulent channel flow[3–7] and pipe flow[1,8–10] of a drag-reducing polymer solution, experimental studies on turbulent channel flow[11–15] and pipe flow[16–19] involving a drag-reducing surfactant solution have yielded valuable knowledge about the attenuation of turbulence, the modification of near-wall coherent structures such as low-speed streaks and quasistreamwise vortices, and the stress defect in which the sum of viscous and turbulent shear stresses is not equal to the total shear stress. However, there have been no studies on the effect of a drag-reducing surfactant solution on a turbulent boundary layer, which is a typical external flow, while for a turbulent boundary layer with a drag-reducing polymer solution, Koskie and Tiederman[20] and White, Somandepalli, and Mungal[21] clarified its velocity profile using laser-Doppler velocimetry (LDV) and particle image velocimetry (PIV), respectively.

The rheological properties of surfactant and polymer solutions are generally similar, since the behavior of worm-like micelle solutions is similar to that of polymer solutions. However, the micelles, which are in a state of thermodynamic equilibrium within the solvent, can be continuously broken and reformed, unlike a covalently bonded polymer backbone.[2,22] Therefore, a surfactant can be a promising drag-reducing additive for some applications, and has actually been utilized in a district's heating and cooling systems to reduce pumping power.[2] Related studies on this heat-transferring ability of drag-reducing surfactant solutions have been done.[23–25] The other noteworthy rheological property of surfactant solutions is that the viscoelastic effect appears only when shear rate becomes larger than a certain critical value, unlike polymer solutions.[2,22] Since turbulent and potential flows are mixing in a turbulent boundary layer flow, which is totally different from an internal flow, a study of the turbulent boundary-layer mixing of turbulent and potential flows in a surfactant solution will be helpful for understanding the mechanism of drag reduction, a process which cannot be learned from studies of internal turbulent flows (i.e., turbulent channel and pipe flows) with surfactant solutions or from turbulent boundary layer flows with polymer solutions.

In the last decade, with the rapid growth of computational resources, direct numerical simulation (DNS) has been performed to investigate the drag-reducing turbulent flows of viscoelastic fluids. There have been a lot of studies on DNS of turbulent channel flow[15,26–34] and turbulent pipe flow[9] using constitutive equation models such as Oldroyd-B, Giesekus, and finitely extensible nonlinear elastic-Peterlin (FENE-P), while there are few studies or experiments on turbulent boundary layer flow. Quite recently, Dimitropoulos, Dubief, Shaqfeh, Moin, and Lele[35] performed a DNS of a polymer-induced drag-reducing zero-pressure gradient turbulent boundary layer flow using the FENE-P model. DNS (Ref. 35) can predict the experimental measurements[21] on a developing boundary layer in polymer solutions, but it does

[a)]Author to whom correspondence should be addressed. Telephone: +81 52 735 5328. Fax: +81 52 735 5247. Electronic mail: itoh.motoyuki@nitech.ac.jp

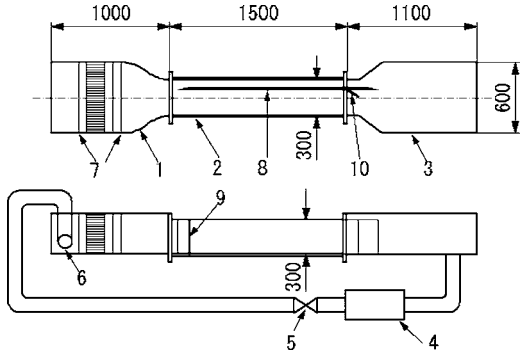

FIG. 1. Experimental apparatus. 1—inlet tank, 2—acrylic channel, 3—outlet tank, 4—centrifugal pump, 5—valve, 6—distribution manifold, 7—flow straightener, 8—test plate, 9—trip wire, 10—flap.

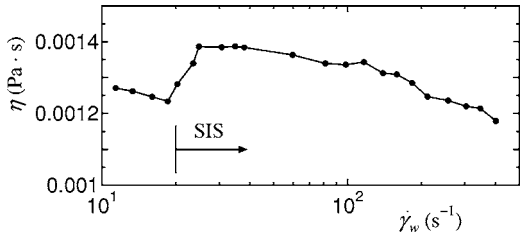

FIG. 2. Shear viscosity as a function of the shear rate: C_{16}TASal, 75 ppm, $T=20.0$ °C.

not deal with the drag-reducing turbulent boundary layer in surfactant solutions.

In the present study, the mean velocity and turbulence statistics in a zero-pressure gradient turbulent boundary layer of a drag-reducing surfactant solution were measured using a two-component LDV system. The results obtained are compared with the corresponding statistics for water.

II. EXPERIMENTAL APPARATUS AND PROCEDURE

The experiments were conducted in a closed-loop water tunnel with a cross section of 300×300 mm and a length of 1500 mm in which a test plate of $20\times295\times1700$ mm was installed, where the test plate was perpendicular to the bottom surface of the acrylic channel (see Fig. 1). All parts in contact with the surfactant solution were made of acrylic resin or stainless steel. A 2-mm diameter trip wire was fixed 100-mm downstream from the leading edge to assure a consistent transition location. The difference in free-stream velocities ($U_e\simeq300$ mm/s) between the location of the leading edge of the test plate and the location 1000-mm downstream was less than 1%, where the flap was used for the zero-pressure gradient turbulent boundary layer. The working fluids were circulated by a stainless steel centrifugal pump. The turbulence and spatial irregularities of the flow were reduced by passing through porous plates, honeycombs, and mesh screens. After that, the flow was uniformed by a convergent nozzle. We also confirmed that the free-stream turbulence intensity was less than 2%.

The surfactant solution (C_{16}TASal) used here was a mixture of cetyltrimethyl ammonium bromide with sodium salicylate as counterion, which was dissolved in de-ionized water. The concentration was 75 ppm by weight in this study.

The two-component LDV system (300-mW argon-ion laser) was used in backscatter mode. The laser light was separated into blue and green beams with wavelengths of 514.5 and 488.0 nm, respectively, and then passed through the bottom of the channel. The measuring volumes are 0.072×0.864 mm for the green beams and 0.068×0.824 mm for the blue beams. The probe was slightly tilted (5°) with respect to the test plate surface in order to measure velocity very close to the wall. The flow was seeded with nylon powder particles (mean diameter: 4.1 μm and specific gravity: 1.02). LDV measurements under free-stream velocity $U_e\simeq300$ mm/s and fluid temperature $T=20.0\pm0.1$ °C were made at the location of 150-mm height from the channel bottom, and at locations downstream from the leading edge where $x=300$, 500, 800, or 1000 mm. Typical data rates in the locations away from the wall were about 300 Hz, falling off to about 20 Hz very close to the wall. Data samples in the locations away from and near the wall were about 25 000 and 5 000, respectively. These values are almost the same as those of Ching, Djenidi, and Antonia.[36]

III. RESULTS AND DISCUSSION

A. Shear viscosity

Shear viscosity η of the surfactant solution was measured at temperature $T=20.0\pm0.2$ °C using a homemade capillary viscometer with an internal diameter of 5.07 mm. Figure 2 shows that the shear viscosity suddenly increased at the shear rate $\dot{\gamma}_w\simeq20$ s^{-1} by a factor of about 1.4 compared with that of water. This phenomena is called the shear-induced state (SIS).[2] Shear thinning can also be observed where the shear viscosity decreases gradually with an increase in shear rate. It has been suggested that SIS is strongly related to drag reduction in the turbulent flow of surfactant

TABLE I. Boundary layer parameters and friction velocity.

	C_{16}TASal (75 ppm)				Water			
x (mm)	δ (mm)	δ^* (mm)	θ (mm)	u_τ (mm/s)	δ (mm)	δ^* (mm)	θ (mm)	u_τ (mm/s)
300	12.7	2.91	1.63	13.2	14.8	3.15	2.14	15.3
500	16.8	3.71	2.04	10.6	22.7	3.94	2.72	15.0
800	20.5	4.50	2.47	9.5	29.1	4.82	3.36	14.3
1000	23.0	4.87	2.65	8.5	33.0	5.38	3.78	13.9

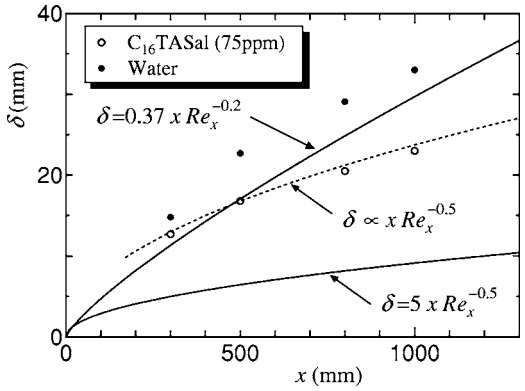

FIG. 3. Development of boundary layer thickness.

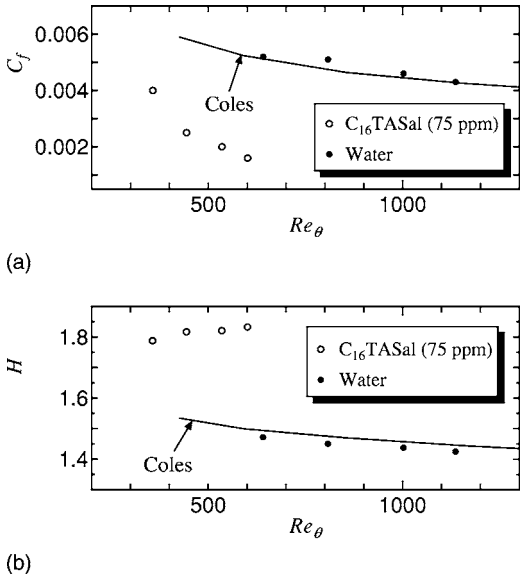

FIG. 4. Streamwise evolution of the boundary layer: (a) friction coefficient, (b) shape factor.

solutions, since in SIS, the rod-like micelles form large structures that can directly affect turbulence structures.

B. Boundary layer parameters

Typical boundary layer parameters such as boundary layer thickness δ, displacement thickness δ^*, momentum thickness θ, and the friction velocity u_τ at $x=300$, 500, 800, and 1000 mm are shown in Table I for the surfactant solution and water. The friction velocity u_τ was obtained by estimating the wall shear stress from the mean velocity gradient, the shear viscosity at the wall for the surfactant solution, and by the Clauser method for water. We confirmed that the value of u_τ obtained by the Clauser method for water was almost the same as that estimated by the mean velocity gradient. The length scales δ, δ^*, and θ for the surfactant solutions are smaller than those for water at the same streamwise location x, respectively. Recently, Suzuki, Fuller, Nakayama, and Usui[37] reported that the boundary layer development for surfactant solutions was characterized by laminar flow, i.e., $\delta \propto x^{0.5}$. In the present study (Fig. 3), the dependence of δ on x for the surfactant solution is similar to that of the Newtonian laminar flow ($\delta \propto x\,\mathrm{Re}_x^{-0.5} \propto x^{0.5}$), rather than that of the Newtonian turbulent flow[38] ($\delta = 0.37x\,\mathrm{Re}_x^{-0.2} \propto x^{0.8}$). However, the boundary layer thickness for surfactant solutions is very different from that of the Blasius laminar law ($\delta = 5x\,\mathrm{Re}_x^{-0.5}$), since the turbulent boundary layer in the present study was tripped at $x=100$ mm.

As the nondimensional parameters of the boundary layer, the friction coefficient $C_f = 2(u_\tau/U_e)^2$, shape factor $H = \delta^*/\theta$, momentum-thickness Reynolds number $\mathrm{Re}_\theta = U_e\theta/\nu$, and surface-length Reynolds number $\mathrm{Re}_x = U_e x/\nu$ are shown in Table II for the surfactant solution and water. The kinematic viscosity ν for surfactant solution was determined using the shear rate at the wall. Figures 4(a) and 4(b) show the dependence of the friction coefficient C_f and shape factor H on the momentum-thickness Reynolds number Re_θ, respectively. In these figures, the solid lines represent Coles' curves.[39] The data of C_f and H for water agree well with Coles' curves. The values of H for the surfactant solution are larger than those for water, and they are between the value for the laminar flow ($H=2.59$) and the values for the turbulent flow of Newtonian fluid. For the surfactant solution, the value of H increases with the increase of Re_θ, while it decreases for water. The drag reduction ratio %DR is also shown in Table II, which is defined as follows:

$$\%\mathrm{DR} = (C_{f,\mathrm{water}} - C_{f,\mathrm{surfactant}})/C_{f,\mathrm{water}} \times 100, \tag{1}$$

under the conditions of the same positions and free-stream velocity. The uncertainty in %DR was estimated at ±5% of its absolute value. Figure 5 shows that the shape factor H increases with increasing drag reduction. In the present experiments, the following relation between the shape factor H and the drag reduction ratio %DR is obtained:

$$H = 0.0012(\%\mathrm{DR}) + 1.755. \tag{2}$$

TABLE II. Nondimensional parameters of boundary layer.

	C_{16}TASal (75 ppm)				Water				
x (mm)	C_f	H	Re_θ	Re_x	C_f	H	Re_θ	Re_x	%DR
300	4.0×10^{-3}	1.788	357	6.58×10^4	5.2×10^{-3}	1.472	641	8.99×10^4	25.6
500	2.5×10^{-3}	1.817	444	1.09×10^5	5.1×10^{-3}	1.451	808	1.49×10^5	50.1
800	2.0×10^{-3}	1.821	535	1.77×10^5	4.6×10^{-3}	1.438	1002	2.38×10^5	55.8
1000	1.6×10^{-3}	1.833	601	2.25×10^5	4.3×10^{-3}	1.425	1136	3.01×10^5	62.6

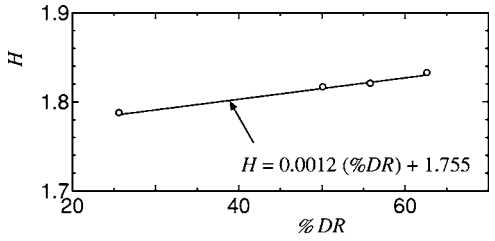

FIG. 5. Shape factor vs drag reduction.

C. Mean velocity

The distribution of the mean velocity scaled by the free-stream velocity U/U_e is shown in Fig. 6. The measurements of U/U_e for surfactant solutions are presented at the locations of $x=300$, 500, 800, and 1000 mm, while the data for water are plotted only at $x=300$ and 1000 mm. The solid and dashed lines in the figure represent $1/n$th-power law ($n=6$) and the Blasius laminar profile,[38] respectively. The mean velocities U/U_e near the wall ($y/\delta \leqslant 0.2$) for the surfactant solution, whose profiles are collapsed for the different Reynolds numbers Re_θ, are about in the middle between the mean velocity profile of water and the Blasius laminar profile.

Figure 7 shows the profiles of the mean velocity $U^+ = U/u_\tau$ in the wall-coordinate $y^+ = u_\tau y/\nu$. It is seen that the present data for water collapse on the log-law profile ($U^+ = 2.44 \ln y^+ + 5.0$). The value of U^+ for the surfactant solution increases with increasing Re_θ, namely, with increasing the amount of drag reduction. Although it is known that the mean velocity U^+ can be larger than Virk's ultimate profile ($U^+ = 11.7 \ln y^+ - 17$)[1] in the maximum drag-reducing flow of surfactant solutions,[12,17] the mean velocity U^+ in the present study does not exceed Virk's ultimate profile even in the largest drag-reduction case (%DR=62.6, Re_θ=601).

To investigate the mean velocity profile in detail, the profile of $y^+ dU^+/dy^+$, which is obtained by the B-spline interpolation, is shown in Fig. 8. The region where the value of $y^+ dU^+/dy^+$ is constant corresponds to the logarithmic region,

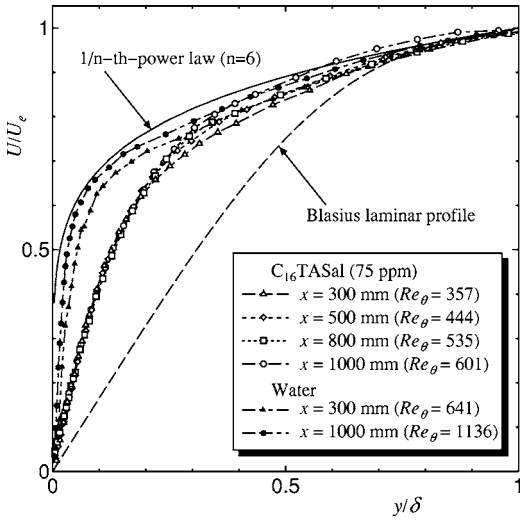

FIG. 6. Mean velocity distribution.

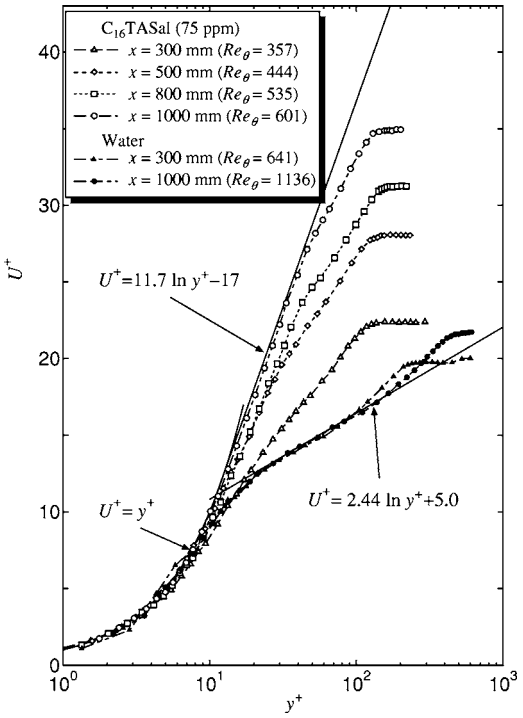

FIG. 7. Mean velocity distribution in wall coordinates.

and its constant value is the inverse of the Kármán constant. For water at Re_θ=641, the value of $y^+ dU^+/dy^+$ is 2.4 at $30 \leqslant y^+ \leqslant 80$. For the surfactant solution at Re_θ=601, two regions of $y^+ dU^+/dy^+ = 12$ and 7.6 appear at $20 \leqslant y^+ \leqslant 30$ and $60 \leqslant y^+ \leqslant 90$, respectively. In the former region, the mean velocity profile collapses on Virk's ultimate profile. The latter region corresponds to the second logarithmic region. We confirmed that the shear rates were about 25 and 10 s^{-1} at $y^+=30$ and 60 (y/δ=0.17 and 0.35), respectively. This indicates that the surfactant solution was in SIS at $y^+ \leqslant 30$ and not in SIS at $y^+ > 60$, respectively (see Fig. 2). In the near-wall region ($y^+ \leqslant 30$) where the slope of the mean velocity profile in Fig. 7 is relatively large, the effect of surfactant additives is apparent, while in the region away from the wall ($y^+ > 60$), where the effect of surfactant additives is rela-

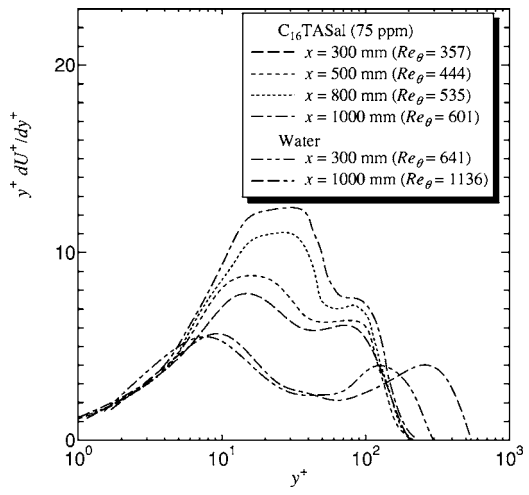

FIG. 8. Distribution of $y^+ dU^+/dy^+$.

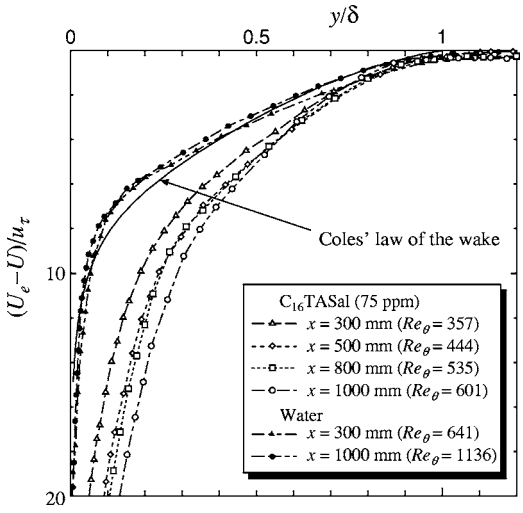

FIG. 9. Velocity defect.

tively small, the slope is smaller than that in the near-wall region, but does not agree with that for water ($y^+dU^+/dy^+ \simeq 7.6 \neq 2.44$). For the surfactant solution at $\mathrm{Re}_\theta = 535$, the value of y^+dU^+/dy^+ is virtually constant at $20 \leqslant y^+ \leqslant 30$ and $50 \leqslant y^+ \leqslant 80$, as well as $\mathrm{Re}_\theta = 601$, while the value of U^+ is smaller than that of Virk's ultimate profile (see Fig. 7). However, the values of y^+dU^+/dy^+ for the surfactant solution at $\mathrm{Re}_\theta = 357$ and 444 are constant only in a single region.

To investigate the velocity defect, the profile of $(U_e - U)/u_\tau$ is shown in Fig. 9. The solid line represents Coles' law of the wake.[40] It was found that the velocity defect becomes gradually larger downstream for a surfactant solution.

D. Turbulence statistics

Distributions of streamwise and wall-normal turbulence intensities scaled by friction velocity $u'^+_{\mathrm{rms}} = \overline{u'^2}^{1/2}/u_\tau$ and $v'^+_{\mathrm{rms}} = \overline{v'^2}^{1/2}/u_\tau$ are shown in Figs. 10(a) and 10(b), respectively, where $'$ represents the turbulent fluctuation with respect to the time average $\overline{(\ )}$. The streamwise turbulence intensity u'^+_{rms} of the surfactant solution increases with an increase of the Reynolds number as reported for the turbulent channel flow of surfactant solutions[12] and for the turbulent boundary layer of polymer solutions.[21] It has been reported that the peak values of u'^+_{rms} for large drag reduction were larger than that for water at high Reynolds numbers, and smaller at low Reynolds numbers in some literature.[6,12,21] The peak of the streamwise turbulence intensity in the present study is smaller than that for water. This may be due to the low Reynolds number effect. The value of y/δ at the maximum of u'^+_{rms} for the surfactant solution is larger than that for water, which is consistent with the fact that the scale of the quasistreamwise vortex for surfactant solutions is larger than that for water (see also Secs. III E and III F), as reported in previous studies.[12–14] It was found that streamwise turbulence intensity distribution has an additional maximum near the center of the boundary layer, where the solution is not locally in SIS due to the effect of the mixing of potential and turbulent flows, in addition to the standard maximum near the wall. This additional maximum has not been previously observed in the turbulent channel flow of surfactant solutions.[12,14] This may be because the large structures of micelles that form near the wall do not disappear suddenly at the center of the channel even if the shear rate there is small enough. The wall-normal turbulence intensity v'^+_{rms} for the surfactant solution is much smaller than that for water and is virtually constant across the boundary layer. In addition, the peak of v'^+_{rms} seen in the canonical wall turbulence does not appear for the surfactant solution. These trends are similar to that of the drag-reducing turbulent channel flow of surfactant solutions.[12,14]

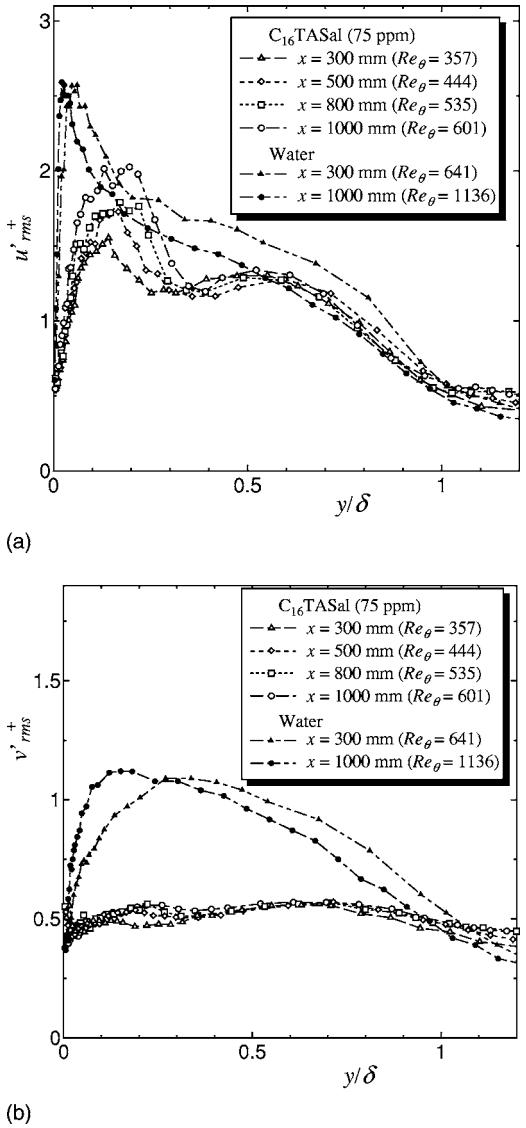

FIG. 10. Distribution of turbulence intensity: (a) streamwise, (b) wall normal.

Figure 11 shows the distributions of Reynolds shear stress scaled by the friction velocity $-\overline{u'v'}^+ = -\overline{u'v'}/u_\tau^2$. Reynolds shear stress for the surfactant solution, which is much smaller than that for water, has a slight maximum near the center of the boundary layer, which corresponds to the maximum observed in the profile of the streamwise turbulence intensity [see Fig. 10(a)]. It has not been reported that the maximum of the Reynolds shear stress near the center of the

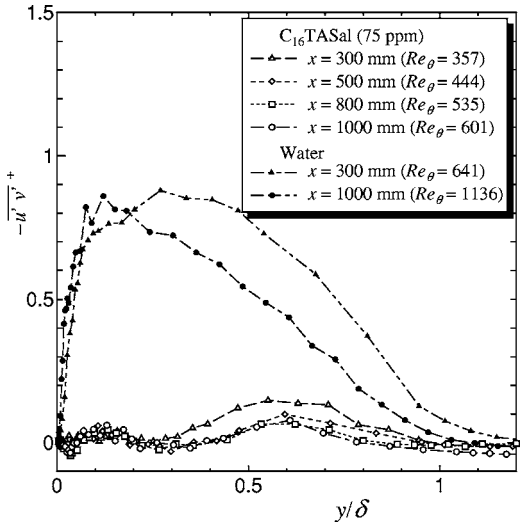

FIG. 11. Distribution of Reynolds shear stress.

boundary layer existed in the drag-reducing turbulent flow. The Reynolds shear stress at $y/\delta \leqslant 0.3$ is almost zero, which is known in the drag-reducing turbulent channel flow in surfactant solutions.[12,14]

The distribution of the correlation coefficient of the streamwise and wall-normal turbulent fluctuations,

$$R_{u'v'} = \frac{-\overline{u'v'}}{u'_{\mathrm{rms}} v'_{\mathrm{rms}}}, \tag{3}$$

is shown in Fig. 12. It was found that the difference in the correlation coefficient $R_{u'v'}$ between the surfactant solution and water was smaller than that in the Reynolds shear stress $-\overline{u'v'}^{+}$.

E. Higher-order statistics

Higher-order turbulence statistics, i.e., the skewness and flatness factors, are useful in understanding near-wall turbulence structures of wall-bounded turbulent flow, since they

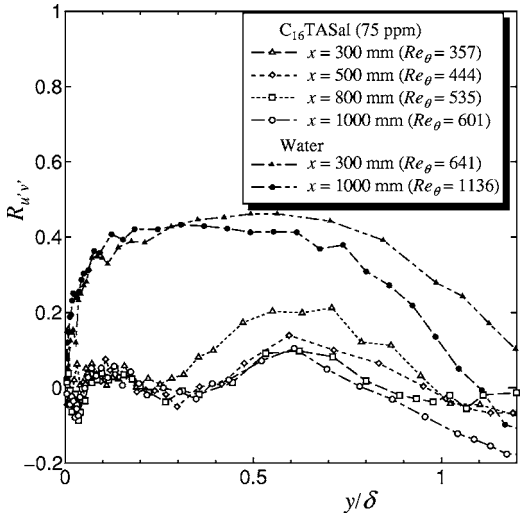

FIG. 12. Distribution of correlation coefficient of streamwise and wall-normal turbulent fluctuations.

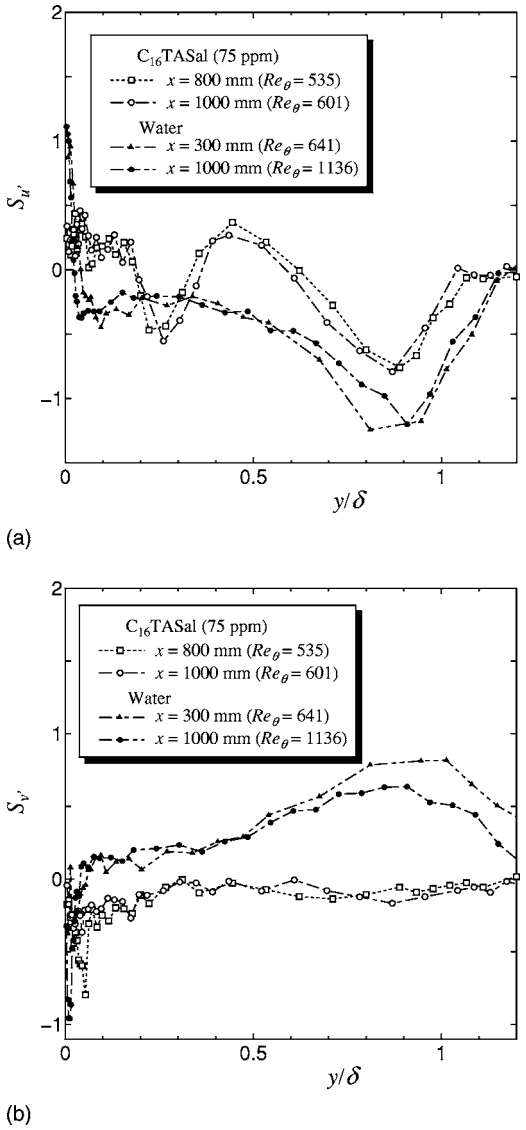

FIG. 13. Skewness factor of turbulent fluctuation: (a) streamwise, (b) wall normal.

are closely related to turbulence structures. For drag-reducing turbulent flow, however, our knowledge of higher-order turbulence statistics remains insufficient.[5,9] The skewness factors of the streamwise and wall-normal turbulent fluctuations, $S_{u'}=\overline{u'^3}/(u')^3_{\mathrm{rms}}$ and $S_{v'}=\overline{v'^3}/(v')^3_{\mathrm{rms}}$, are shown in Figs. 13(a) and 13(b), respectively. In addition, the flatness factors of the streamwise and wall-normal velocity fluctuations, $F_{u'}=\overline{u'^4}/(u')^4_{\mathrm{rms}}$ and $F_{v'}=\overline{v'^4}/(v')^4_{\mathrm{rms}}$, are shown in Figs. 14(a) and 14(b), respectively. The maximum of $S_{u'}$ appears at $y/\delta \simeq 0.5$ for the surfactant solution, but this was not seen for water. It was also found that the skewness and flatness factors $S_{v'}$ and $F_{v'}$ are virtually constant ($S_{v'} \simeq 0$, $F_{v'} \simeq 3.5$) across the turbulent boundary layer for the surfactant solution.

Figure 15 shows the distributions of the streamwise turbulence intensity u'^{+}_{rms}, skewness and flatness factors of streamwise velocity fluctuations, $S_{u'}$ and $F_{u'}$, for both the surfactant solution for $\mathrm{Re}_\theta=601$ and water for $\mathrm{Re}_\theta=641$. In this figure, the dashed line (a) represents the location of $S_{u'}$

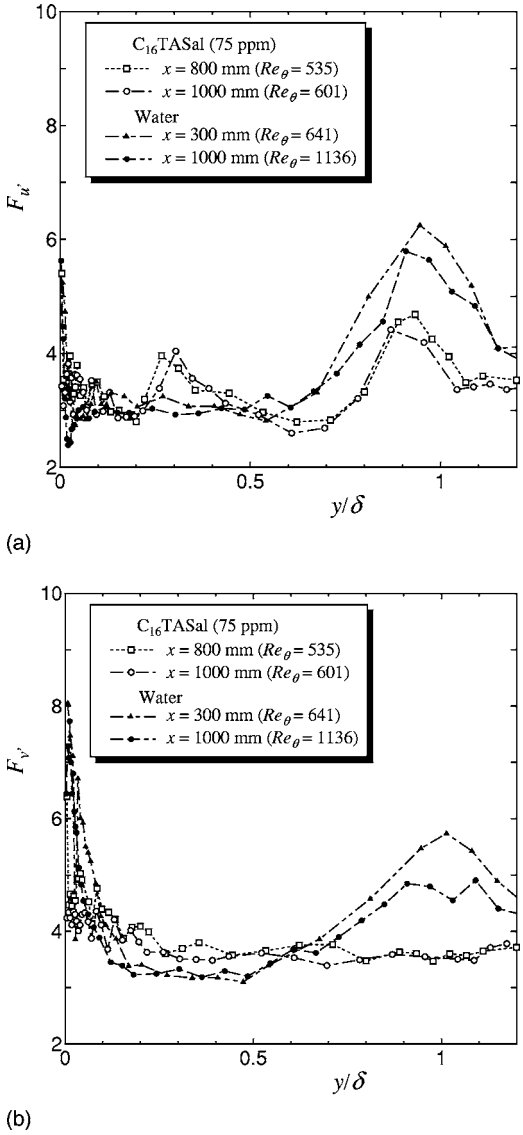

FIG. 14. Flatness factor of turbulent fluctuation: (a) streamwise, (b) wall normal.

=0 for water, while dashed lines (b)–(d) represent the locations of $S_{u'}=0$ for surfactant solutions. For the water at location (a) ($y/\delta=0.04$, $y^+\simeq 10$), the streamwise turbulence intensity u'^+_{rms} and flatness factor $F_{u'}$ have the maximum and minimum, respectively, This relationship for water observed at location (a) corresponds to that for the surfactant solutions at location (b) ($y/\delta=0.19$, $y^+\simeq 30$). Here the value of y/δ at location (b) is larger than that at location (a), which indicates that the scale of the quasistreamwise vortex for the surfactant solution is larger than that for water, as seen in turbulent channel flow.[12,13] For the surfactant solution at location (c) ($y/\delta=0.36$, $y^+\simeq 60$), the streamwise turbulence intensity profile has a minimum. The location of $y^+\simeq 60$ corresponds to the location of the lower end in the logarithmic region (see Fig. 8). In addition, for the surfactant solution at location (d) ($y/\delta=0.59$, $y^+\simeq 100$), the streamwise turbulence intensity u'^+_{rms} has an additional maximum, where the Reynolds shear stress has a corresponding maximum, and the flatness factor $F_{u'}$ has a corresponding minimum, respectively. It is noticeable that the relationship between streamwise turbulence intensity and the flatness factor for the surfactant solution at location (d) is equal to that for water at location (a) and to that for the surfactant solution at location (b).

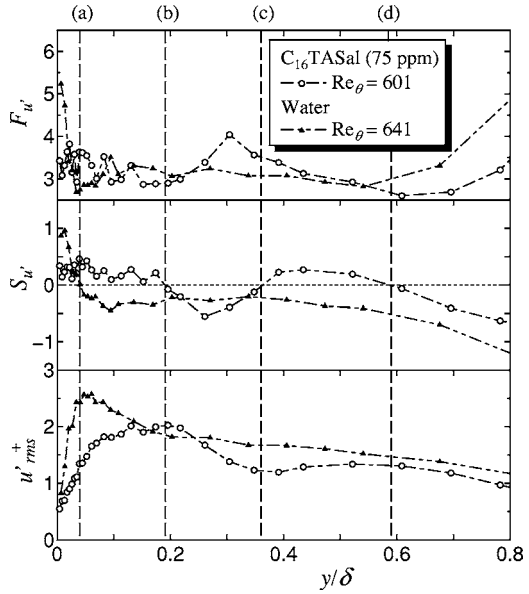

FIG. 15. Turbulence intensity, skewness, and flatness factors of streamwise turbulent fluctuation.

F. Power spectra

The power spectra of the streamwise velocity fluctuations scaled by the mean square of the velocity fluctuations $P_u(f)/\overline{u'^2}$ at $y/\delta=0.2$ and $y/\delta=0.6$ are shown in Figs. 16(a) and 16(b), respectively. The locations of $y/\delta=0.2$ and $y/\delta=0.6$ correspond to the regions close to the standard and additional maxima of the streamwise turbulence intensity for the surfactant solution, respectively. For simplicity, the data are plotted only at $x=300$ and 1000 mm for both the surfactant solution and water. At low frequencies, the power spectrum for the surfactant solution ($\mathrm{Re}_\theta=601$) is larger than that for water ($\mathrm{Re}_\theta=641$) at both $y/\delta=0.2$ and 0.6, as well as for the drag-reducing turbulent channel flow.[6,12] This is consistent in that the structure of the quasistreamwise vortex becomes larger for the surfactant solution (see Sec. III E). Comparing the power spectra of $\mathrm{Re}_\theta=351$ and 601 for the surfactant solution, the power spectrum at low frequencies increases with an increase in the momentum-thickness Reynolds number Re_θ, namely, the drag reduction ratio %DR.

IV. CONCLUSION AND DISCUSSION

The influence of a drag-reducing surfactant on a zero-pressure gradient turbulent boundary layer was investigated using a two-component LDV system. LDV measurements were made for four different momentum-thickness Reynolds numbers, $\mathrm{Re}_\theta=357$, 444, 535, and 601. The amount of drag reduction was from 25.6% to 62.6% when compared to a water flow at the same position and free-stream velocity. The present study is summarized as follows.

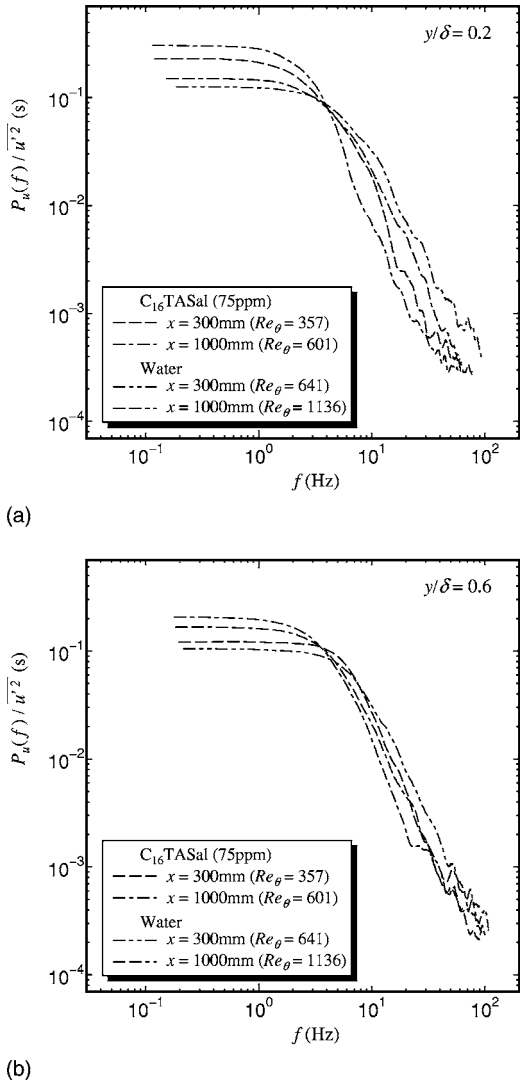

FIG. 16. Power spectra of streamwise velocity fluctuation: (a) at $y/\delta=0.2$, (b) at $y/\delta=0.6$.

For the surfactant solution, the value of the shape factor increases with an increase in the momentum-thickness Reynolds number, while it decreases for water. The mean velocities scaled by the free-stream velocity near the wall for the surfactant solution, whose profiles are collapsed for the different Reynolds numbers Re_θ, are about in the middle between the mean velocity profile of water and the Blasius laminar profile. The mean velocity distribution in wall coordinates indicates the existence of two logarithmic regions for large drag-reduction cases. It was found that the streamwise turbulence intensity distribution had an additional maximum near the center of the boundary layer, where the surfactant solution was not locally in SIS due to the effect of the mixing of potential and turbulent flows, as not seen in the turbulent channel flow of surfactant solutions nor in the turbulent boundary layer flow of polymer solutions. The location of the additional maximum of streamwise turbulence intensity corresponds to the location at which the Reynolds shear stress has a slight maximum, the skewness factor of streamwise turbulent fluctuation is zero, and the flatness factor has a corresponding minimum. It was also found that wall-normal turbulence intensity and skewness and flatness factors of wall-normal turbulent fluctuations were virtually constant across the turbulent boundary layer for the surfactant solution.

The results of the present study provide various data not observed in the turbulent channel and pipe flows of surfactant solutions nor in the turbulent boundary layer flows of polymer solutions. However, it remains unknown whether the drag reduction in surfactant solutions is attributable to the large structure of rod-like micelles or the resultant viscoelastic effect, since it is very difficult to obtain information on the large structure of rod-like micelles in the turbulent boundary layer flow. However, the effect of macromolecular polymer structures on drag reduction has been recently investigated using a birefringence measurement.[41] In addition, it is difficult to correctly measure viscoelastic properties[42] such as the first normal stress difference or extensional viscosity for the dilute surfactant solutions used in the present study. It has been reported that the drag-reducing surfactant solution in which the network of rod-like micelles was formed did not necessarily have viscoelasticity.[43,44] Recently, drag reductions of up to 26% were obtained by numerical simulation of turbulent drag reduction using rigid fibers.[45] This indicates that elasticity is not necessary to achieve turbulent drag reduction. As an alternative to a viscoelastic mechanism, an electrokinetic mechanism[46] has been proposed to explain the drag reduction of turbulent flow in surfactant solutions. An investigation on the drag-reducing mechanism for surfactant solutions is indeed required, but this study shows that the large structures of rod-like micelles are likely to be the key factor causing drag reduction in the turbulent flow of surfactant solutions, although it remains unknown whether such large structures directly connect with the drag reduction or not.

[1] P. S. Virk, "Drag reduction fundamentals," AIChE J. **21**, 625 (1975).
[2] A. Gyr and H.-W. Bewersdorff, *Drag Reduction of Turbulent Flows by Additives* (Kluwer, Dordrecht, The Netherlands, 1995).
[3] T. S. Luchik and W. G. Tiederman, "Turbulent structure in low-concentration drag-reducing channel flows," J. Fluid Mech. **190**, 241 (1988).
[4] D. T. Walker and W. G. Tiederman, "Turbulent structure in a channel flow with polymer injection at the wall," J. Fluid Mech. **218**, 377 (1990).
[5] T. Wei and W. W. Willmarth, "Modifying turbulent structure with drag-reducing polymer additives in turbulent channel flows," J. Fluid Mech. **245**, 619 (1992).
[6] M. D. Warholic, H. Massah, and T. J. Hanratty, "Influence of drag-reducing polymers on turbulence: Effects of Reynolds number, concentration and mixing," Exp. Fluids **27**, 461 (1999).
[7] M. D. Warholic, D. K. Heist, M. Katcher, and T. J. Hanratty, "A study with particle-image velocimetry of the influence of drag-reducing polymers on the structure of turbulence," Exp. Fluids **31**, 474 (2001).
[8] H. Usui, K. Maeguchi, and Y. Sano, "Drag reduction caused by the injection of polymer thread into a turbulent pipe flow," Phys. Fluids **31**, 2518 (1988).
[9] J. M. J. Den Toonder, M. A. Hulsen, G. D. C. Kuiken, and F. T. M. Nieuwstadt, "Drag reduction by polymer additives in a turbulent pipe flow: Numerical and laboratory experiments," J. Fluid Mech. **337**, 193 (1997).
[10] P. K. Ptasinski, F. T. M. Nieuwstadt, B. H. A. A. Van den Brule, and M. A. Hulsen, "Experiments in turbulent pipe flow with polymer additives at maximum drag reduction," Flow, Turbul. Combust. **66**, 159 (2001).
[11] M. Itoh, S. Imao, and K. Sugiyama, "Characteristics of low-speed streaks in the flow of drag-reducing surfactant solution," JSME Int. J., Ser. B **40**, 550 (1997).

[12]M. D. Warholic, G. M. Schmidt, and T. J. Hanratty, "The influence of a drag-reducing surfactant on a turbulent velocity field," J. Fluid Mech. **388**, 1 (1999).
[13]M. Itoh and Y. Kurokawa, "Visualization of turbulent structure in the drag-reducing flow of aqueous surfactant solution," Proceedings of the 14th Australasian Fluid Mechanics Conference, Adelaide University, Adelaide, Australia, 10–14 December 2001, pp. 877–880.
[14]Y. Kawaguchi, T. Segawa, Z. Feng, and P. Li, "Experimental study on drag-reducing channel flow with surfactant additives–spatial structure of turbulence investigated by PIV system," Int. J. Heat Mass Transfer **23**, 700 (2002).
[15]B. Yu, F. Li, and Y. Kawaguchi, "Numerical and experimental investigation of turbulent characteristics in a drag-reducing flow with surfactant additives," Int. J. Heat Mass Transfer **25**, 961 (2004).
[16]H.-W. Bewersdorff, in *Structure of Turbulence and Drag Reduction*, edited by A. Gyr (Springer, Berlin, 1990), pp. 293–312.
[17]Z. Chara, J. L. Zakin, M. Severa, and J. Myska, "Turbulence measurements of drag reducing surfactant systems," Exp. Fluids **16**, 36 (1993).
[18]G. Hetsroni, J. L. Zakin, and A. Mosyak, "Low-speed streak in drag-reduced turbulent flow," Phys. Fluids **9**, 2397 (1997).
[19]M. Nowak, "Time-dependent drag reduction and ageing in aqueous solutions of a cationic surfactant," Exp. Fluids **34**, 397 (2003).
[20]J. Koskie and W. G. Tiederman, "Polymer drag reduction of a zero-pressure-gradient boundary layer," Phys. Fluids A **3**, 2471 (1991).
[21]C. M. White, V. S. R. Somandepalli, and M. G. Mungal, "The turbulence structure of drag-reduced boundary layer flow," Exp. Fluids **36**, 62 (2004).
[22]S. Chen and J. P. Rothstein, "Flow of a wormlike micelle solution past a falling sphere," J. Non-Newtonian Fluid Mech. **116**, 205 (2004).
[23]Y. Qi, Y. Kawaguchi, R. N. Christensen, and J. L. Zakin, "Enhancing heat transfer ability of drag reducing surfactant solutions with static mixers and honeycombs," Int. J. Heat Mass Transfer **46**, 5161 (2003).
[24]Y. Qi, L. K. Weavers, and J. L. Zakin, "Enhancing heat-transfer ability of drag reducing surfactant solutions with ultrasonic energy," J. Non-Newtonian Fluid Mech. **116**, 71 (2003).
[25]F.-C. Li, Y. Kawaguchi, and K. Hishida, "Investigation on the characteristics of turbulence transport for momentum and heat in a drag-reducing surfactant solution flow," Phys. Fluids **16**, 3281 (2004).
[26]R. Sureshkumar, A. N. Beris, and R. A. Handler, "Direct numerical simulation of the turbulent channel flow of a polymer solution," Phys. Fluids **9**, 743 (1997).
[27]C. D. Dimitropoulos, R. Sureshkumar, A. N. Beris, and R. A. Handler, "Budgets of Reynolds stress, kinetic energy and streamwise enstrophy in viscoelastic turbulent channel flow," Phys. Fluids **13**, 1016 (2001).
[28]S. Sibilla and A. Baron, "Polymer stress statistics in the near-wall turbulent flow of a drag-reducing solution," Phys. Fluids **14**, 1123 (2002).
[29]T. Min, J. Y. Yoo, H. Choi, and D. D. Joseph, "Drag reduction by polymer additives in a turbulent channel flow," J. Fluid Mech. **486**, 213 (2003).
[30]P. K. Ptasinski, B. J. Boersma, F. T. M. Nieuwstadt, M. A. Hulsen, B. H. A. A. Van den Brule, and J. C. R. Hunt, "Turbulent channel flow near maximum drag reduction: Simulations, experiments, and mechanisms," J. Fluid Mech. **490**, 251 (2003).
[31]T. Min, H. Choi, and J. Y. Yoo, "Maximum drag reduction in a turbulent channel flow by polymer additives," J. Fluid Mech. **492**, 91 (2003).
[32]B. Yu and Y. Kawaguchi, "Effect of Weissenberg number on the flow structure: DNS study of drag-reducing flow with surfactant additives," Int. J. Heat Fluid Flow **24**, 491 (2003).
[33]B. Yu and Y. Kawaguchi, "Direct numerical simulation of viscoelastic drag-reducing flow: A faithful finite difference method," J. Non-Newtonian Fluid Mech. **116**, 431 (2004).
[34]Y. Dubief, C. M. White, V. E. Terrapon, E. S. G. Shaqfeh, P. Moin, and S. K. Lele, "On the coherent drag-reducing and turbulence-enhancing behaviour of polymers in wall flows," J. Fluid Mech. **514**, 271 (2004).
[35]C. D. Dimitropoulos, Y. Dubief, E. S. G. Shaqfeh, P. Moin, and S. K. Lele, "Direct numerical simulation of polymer-induced drag reduction in turbulent boundary layer flow," Phys. Fluids **17**, 011702 (2005).
[36]C. Y. Ching, L. Djenidi, and A. Antonia, "Low-Reynolds-number effects in a turbulent boundary layer," Exp. Fluids **19**, 61 (1995).
[37]H. Suzuki, G. G. Fuller, T. Nakayama, and H. Usui, "Development characteristics of drag-reducing surfactant solution flow in a duct," Rheol. Acta **43**, 232 (2004).
[38]H. Schlichting, *Boundary-Layer Theory*, 7th ed. (McGraw-Hill, New York, 1979).
[39]D. E. Coles, "The turbulent boundary layer in a compressible fluid," Report No. R-403-PR, The Rand Corp., Santa Monica, CA, 1962.
[40]D. E. Coles, "The law of the wake in the turbulent boundary layer," J. Fluid Mech. **1**, 191 (1956).
[41]K. Kim, M. T. Islam, X. Shen, A. I. Sirviente, and M. J. Solomon, "Effect of macromolecular polymer structures on drag reduction in a turbulent channel flow," Phys. Fluids **16**, 4150 (2004).
[42]Y. Kawaguchi, J.-J. Wei, B. Yu, and Z.-P. Feng, "Rheological characterization of drag-reducing cationic surfactant—shear and elongational viscosities of dilute solutions," Proceedings of the Fourth American Society of Mechanical Engineering–Japan Society of Mechanical Engineers (ASME-JSME) Joint Fluids Engineering Conference, Honolulu, HI, 6–10 July 2003, FEDSM2003-45653.
[43]B. Lu, X. Li, J. L. Zakin, and Y. Talmon, "A non-viscoelastic drag reducing cationic surfactant system," J. Non-Newtonian Fluid Mech. **71**, 59 (1997).
[44]Z. Lin, Y. Zheng, H. T. Davis, L. E. Scriven, Y. Talmon, and J. L. Zakin, "Unusual effects of counterion to surfactant concentration ratio on viscoelasticity of a cationic surfactant drag reducer," J. Non-Newtonian Fluid Mech. **93**, 363 (2000).
[45]J. S. Paschkewitz, Y. Dubief, C. D. Dimitropoulos, E. S. G. Shaqfeh, and P. Moin, "Numerical simulation of turbulent drag reduction using rigid fibres," J. Fluid Mech. **518**, 281 (2004).
[46]M. Fichman and G. Hetsroni, "Electrokinetic aspects of turbulent drag reduction in surfactant solutions," Phys. Fluids **16**, 4346 (2004).